AJ Accepted
Preprint typeset using LaTeX style emulateapj v. 10/09/06

WIDE-FIELD SURVEY AROUND LOCAL GROUP DWARF SPHEROIDAL GALAXY LEO II: SPATIAL DISTRIBUTION OF STELLAR CONTENT[1]

Yutaka Komiyama,[2,3] Mamoru Doi,[4] Hisanori Furusawa,[3] Masaru Hamabe,[5] Katsumi Imi, Masahiko Kimura,[3] Satoshi Miyazaki,[3] Fumiaki Nakata,[2] Norio Okada,[2] Sadanori Okamura,[6,7] Masami Ouchi,[8,9] Maki Sekiguchi, Kazuhiro Shimasaku,[6,7] Masafumi Yagi,[2] and Naoki Yasuda[10]

AJ Accepted

ABSTRACT

We carried out a wide-field V, I imaging survey of the Local Group dwarf spheroidal galaxy Leo II using the Subaru Prime Focus Camera on the 8.2-m Subaru Telescope. The survey covered an area of 26.67×26.67 arcmin^2, far beyond the tidal radius of Leo II (8.63 arcmin), down to the limiting magnitude of $V \simeq 26$, which is roughly 1 mag deeper than the turn-off point of the main sequence stars of Leo II. Radial number density profiles of bright and faint red giant branch (RGB) stars were found to change their slopes at around the tidal radius, and extend beyond the tidal radius with shallower slopes. A smoothed surface brightness map of Leo II suggests the existence of a small substructure (4×2.5 arcmin^2, 270×170 pc^2 in physical size) of globular cluster luminosity beyond the tidal radius. We investigated the properties of the stellar population by means of the color-magnitude diagram. The horizontal branch (HB) morphology index shows a radial gradient in which red HB stars are more concentrated than blue HB stars, which is common to many Local Group dwarf spheroidal galaxies. The color distribution of RGB stars around the mean RGB sequence shows a larger dispersion at the center than in the outskirts, indicating a mixture of stellar populations at the center and a more homogeneous population in the outskirts. Based on the age estimation using subgiant branch (SGB) stars, we found that although the major star formation took place ~ 8 Gyr ago, a considerable stellar population younger than 8 Gyr is found at the center; such a younger population is insignificant in the outskirts. The following star-formation history is suggested for Leo II. Star-forming activity occurred more than $\gtrsim 8$ Gyr ago throughout the galaxy at a modest star-formation rate. The star-forming region gradually shrank from the outside toward the center and star-forming activity finally dropped to ~ 0 by ~ 4 Gyr ago, except for the center, where a small population younger than 4 Gyr is present.

Subject headings: galaxies: stellar content — galaxies: individual (Leo II) — galaxies: dwarf spheroidal — galaxies: Local Group — galaxies: evolution

1. INTRODUCTION

Dwarf galaxies are the most numerous constituents in the universe and outnumber giant galaxies. In the prevailing hierarchical structure formation scenario (e.g., White & Rees 1978; White & Frenk 1991), they play key roles as building blocks from which larger structures such as giant galaxies are formed. Although most dwarf galaxies contain old stellar populations (Grebel 2000; Grebel & Gallagher 2004), a general trend occurs in the evolution of galaxies in that more massive galaxies are formed at higher redshifts which is known as the "downsizing" effect (Cowie et al. 1996; Smail et al. 1998). It is therefore important to investigate how they evolved over the age of the universe.

Extensive and epoch-making observations of Local Group dwarf galaxies using the Hubble Space Telescope (HST) markedly improved our knowledge of their evolutionary process. These observations have revealed their intriguing star-formation histories, which has been succinctly summarized as "no two Local Group dwarfs have the same star-formation history" (Mateo 1998). However, the Achilles' heel of HST is its small field of view. In the Fornax dwarf spheroidal galaxy, Coleman et al. (2004, 2005) found "lobed" substructures, which are suggested to represent a disrupted merging companion dwarf galaxy located at ~ 1.8 core radii from the center and outside the tidal radius. Evidence for the existence of substructures is also suggested by both photometric and dynamical analyses for Ursa Minor (Kleyna et al. 1998; Wilkinson et al. 2004), Draco (Wilkinson et al. 2004), and Sextans (Kleyna et al. 2004; Walker et al. 2006). Extended halo structures are also found in several close companion dwarf spheroidals of the Milky Way (Ursa Minor, Palma et al. 2003; Carina, Majewski et al. 2005; Sculptor, Westfall et al. 2006), and their origin is often related to the tidal influence of the Milky Way. Regarding stellar populations, da Costa et al. (1996) first pointed out that Leo II, And I and Sculptor show a significant radial gradient in HB morphology. Since then many dwarf spheroidal galaxies have been reported to show ra-

[1] Based on data collected at Subaru Telescope, which is operated by the National Astronomical Observatory of Japan

[2] National Astronomical Observatory of Japan, 2-21-1 Osawa, Mitaka, Tokyo 181-8588, Japan
[3] Subaru Telescope, 650 North Aohoku Place, Hilo, HI 96720, USA
[4] Institute of Astronomy, Graduate School of Science, University of Tokyo, 2-21-1 Osawa, Mitaka, Tokyo 181-0015, Japan
[5] Department of Mathematical and Physical Sciences, Japan Women's University, Bunkyo, Tokyo 112-8681, Japan
[6] Department of Astronomy, University of Tokyo, 7-3-1 Hongo, Bunkyo, Tokyo 113-0033, Japan
[7] Research Center for the Early Universe, School of Science, the University of Tokyo, Bunkyo, Tokyo 113-0033, Japan
[8] Space Telescope Science Institute, Baltimore, MD, USA
[9] Hubble Fellow
[10] Institute for Cosmic Ray Research, University of Tokyo, Kashiwa 277-8582, Japan

dial gradients of stellar populations in the sense of a central concentration of young and metal-rich populations versus more extended metal-poor and old populations (Martínez-Delgado, Gallart & Aparicio 1999; Saviane, Held & Bertelli 2000; Harbeck et al. 2001; Tolstoy et al. 2004). However, some exceptions exist, such as Leo I (Held et al. 2000) and Carina (Smecker-Hane et al. 1994; Harbeck et al 2001), although a mild radial gradient was reported for Carina (Koch et al. 2006). All these results demonstrate that even small dwarf galaxies, often described as simple systems, contain such complex structures inside. Hence, it is important to explore the whole galaxy from this perspective. A combination of good image quality, depth, and a wide field of view is required for such purposes. One of the best facilities for conducting such observations is Suprime-Cam on the 8.2-m Subaru Telescope. We therefore carried out a wide-field imaging survey for the Local Group dwarf spheroidal galaxy Leo II.

Leo II is one of the Milky Way companion dwarf spheroidal galaxies located about 233 kpc from us (Bellazzini et al. 2005). In contrast to the close companion dwarf spheroidal galaxies such as Sextans, Ursa Minor, and Draco, Leo II resides in a relatively remote place from the Milky Way. The stellar content of Leo II was studied extensively by Mighell & Rich (1996) using WFPC2 on HST. They estimated the metallicity of Leo II to be [Fe/H] $= -1.60 \pm 0.25$ based on the V, I color-magnitude diagram, which is consistent with a recent spectroscopic measurement by Bosler et al. (2004) who derived a median metallicity of [Fe/H] $= -1.57$ based on the spectra obtained with Keck LRIS. They also noted that Leo II started forming stars about 14±1 Gyr ago and formed most of its stellar population during the succeeding 7±1 Gyr, with a typical star having formed about 9±1 Gyr ago. A more recent study (Koch et al. 2007) showed that the mean metallicity of Leo II is -1.74 based on the measurement of the calcium triplet for 52 red giants. These investigators also estimated individual ages, and derived a wide age range (2 - 15 Gyr, the same spread as found by Bosler et al. 2004) and an essentially flat age-metallicity relation. Dolphin (2002) reanalyzed the HST data and derived the star-formation history of Leo II. He claimed that the mean metallicity ([Fe/H] $= -1.13$) is higher than the estimates of Mighell & Rich (1996) and Bosler et al. (2004), owing to a young mean age of the stars in Leo II (9.4 Gyr). However, the data are limited to the central small area (4.44 arcmin^2) within the core radius of the galaxy ($2'.9$, Mateo 1998). Recently, Bellazzini et al. (2005) published new V, I photometry data obtained with the 3.5-m TNG covering a relatively wide area of Leo II (9.4×9.4 arcmin^2). They analyzed the spatial variation of the stellar content such as red clump stars and blue HB stars and the magnitude of the AGB bump, which indicates that the main population of Leo II is $\simeq 8$ Gyr. However, their data are shallow ($V_{lim} \sim 22$) and their analysis inevitably limited to features brighter than the HB level. Our data obtained with Suprime-Cam on the 8.2-m Subaru Telescope constitute an excellent data set that gives a crucial clue for understanding the properties of the stellar content of Leo II.

In Section 2, we present the details of our observation and data analysis and show our results in Section 3 through 6. On the basis of these results, we discuss the formation and evolution of Leo II in Section 7 and give a summary in Section 8. Here we adopt the distance modulus of Leo II to be $(m-M)_0 = 21.63$ and the reddening to be $E(B-V) = 0.02$ (Mateo 1998).

2. OBSERVATION AND DATA ANALYSIS

The observation was carried out in April 2001 using the Subaru Prime Focus Camera (Suprime-Cam; Miyazaki et al. 2002) on the 8.2-m Subaru Telescope at Mauna Kea, Hawaii. Suprime-Cam is a wide-field imager consisting of 10 2k×4k CCDs. It covers a sky area of 34×27 arcmin^2 with 0.2 arcsec per pixel sampling. Because of the wide-field coverage and good image quality of the Subaru Telescope, Suprime-Cam is the most powerful instrument for investigating stellar contents of nearby galaxies. We used V and I filters and total exposure times are 3000 sec and 2400 sec in the V and I bands, respectively. Several short exposures were also obtained to measure the luminosities of bright stars, which are saturated in long exposure frames. The sky condition was good and the typical stellar size (FWHM) was about 0.7 arcsec in both V and I bands. The details of the observation are given in Tab. 1.

The data were reduced using the standard data analysis software for Suprime-Cam (Yagi et al. 2002). The reduction procedure is summarized as follows. The bias was subtracted from individual frames and bad pixels were masked. Each frame was divided by the flat frame, which was created from object frames (mostly blank fields) taken in the same observing run. Note that Leo II frames were excluded when creating the flat frames. The optical distortion caused by the prime focus corrector was corrected using an analytical expression of the optical distortion (see Miyazaki et al. 2002), and the sky background was subtracted from each frame. Then the two-dimensional position and the relative brightness of each frame were estimated using common stars found in adjacent CCD chips and different dither positions. Finally we obtained a coadded image. The FWHMs of stars in the resultant coadded images are 0.80 arcsec and 0.78 arcsec in the V and I bands, respectively. We used the central area (8000×8000 pixels, 26.67×26.67 arcmin^2) for the following analysis to guarantee a homogeneous signal-to-noise ratio over the wide field of view. As shown in Fig. 1, the survey area is wide enough and far beyond the tidal radius of Leo II (8.7 arcmin; Mateo 1998).

We applied DAOPHOT PSF photometry software (Stetson 1987, 1994) for the coadded images. The PSF model was made from about 100 stars and we repeated iterations of the PSF photometry three times to not miss faint stars. Non-stellar objects such as galaxies and cosmic rays were excluded using shape and χ^2 parameters calculated by DAOPHOT. Combining bright stellar objects ($V < 20$) detected in short exposure frames and faint stellar objects ($V > 20$) detected in long exposure frames, 82252 objects were cataloged as stellar objects.

Zero-point magnitudes in both V and I bands were calibrated using bright stars ($V < 20$) listed in Lee (1995). We used short exposures for comparison since the bright stars listed in Lee (1995) were saturated in long exposure frames. The zero-point magnitudes are accurate to 0.03 mag and 0.01 mag in the V and I bands, respectively. Long exposure frames were calibrated using common stars (typically 20-22 mag stars) on both long and

short exposure frames. Long exposure frames are accurate to 0.01 mag (relative to short exposures) in both bands.

The magnitude error and the detection completeness were estimated in the standard manner. We divided the 8000×8000 pixel image into 80 × 80 grids consisting of 100×100 pixels. In each grid, an artificial star was added at random position using the `addstar` task in the DAOPHOT package, and the same PSF photometry procedure was applied to the image. This process was repeated for 10 times per every 0.5 magnitude interval for the magnitude ranges of 23.5 mag $< V <$ 26.0 mag and 22.5 mag $< I <$ 25.0 mag, respectively. The magnitude error and the detection completeness were calculated from the result of the PSF photometry for these artificial stars. The result for the V band is shown in Fig. 2 as a function of magnitude and the distance from the galaxy center. The detection completeness is > 0.9 for $V < 24.5$ at any position in the galaxy, but it degrades to 0.6 at the galaxy center for $V = 25.5$. The 90% and 50% completeness limits at the galaxy center are 24.5 and 25.9 in V band, respectively, and those for I band are 22.7 and 24.7, respectively. The magnitude is accurate to 0.02 mag for $V < 24.5$ in most parts of the galaxy, but the degradation is severe at the galaxy center. For $V < 23.5$ and $I < 22.5$, the detection is almost complete and the magnitude is accurate even at the crowded galaxy center.

Fig. 3 shows the color-magnitude diagram of stellar objects found in the central 6.67×6.67 arcmin^2 area of the Leo II field. It is clearly seen that our data cover a wide magnitude range of stars in Leo II from the tip of the RGB ($V \simeq 19$) to the turn-off point ($V \simeq 25$). Remarkable features are the well-defined HB at $V \simeq 22.2$ and the narrow RGB. The red HB is characterized by a concentration of stars at the red side of the RR Lyr instability strip ($0.4 \lesssim V - I \lesssim 0.6$) that is well distinguished from the RGB. The HB extends to the blue side and forms another concentration at $0 \lesssim V - I \lesssim 0.4$. It is obvious that the asymptotic giant branch (AGB) merges into the RGB at $V \sim 21.5$ and the RGB bumps detected by Bellazzini et al. (2005) are clearly seen by eye at $V \sim 21.4$ and $V \sim 21.8$. One might notice that ∼20 stars with the same color as the red HB, but much brighter than the red HB, occur. They may possibly be helium-burning, high-mass stars (Mighell & Rich, 1996; Bellazzini et al. 2005), although Demers & Irwin (1993) first argued that they are a photometric blend of HB and RGB stars. The other noteworthy feature in the color-magnitude diagram is the apparent bifurcation of the blue HB stars. The feature is also seen in Bellazzini et al. (2005; Fig.2), and according to their identification, most of the brighter blue HB stars are variable stars cataloged by Siegel & Majewski (2000). We examined the spatial distribution of these stars and found no particular maldistribution (concentrated or uniform distribution).

We note that the contamination from Galactic stars is not severe compared to other Milky Way satellite galaxies (e.g., Sextans, Draco, and Ursa Minor; See Harbeck et al. 2001) since Leo II is located at a relatively high galactic latitude ($b = 67°$). The contamination becomes severe for $V > 23.5$. The typical photometric errors, which were calculated on the basis of the artificial star test (thus including the effect of the crowding), are plotted as blue (near center) and red (outskirts) error bars in Fig. 4 (a).

3. RADIAL DISTRIBUTION OF THE STELLAR COMPONENT

We first investigated the radial profiles of bright and faint RGB stars and blue and red HB stars. The blue and red HB stars are easily discerned as seen in Fig. 3. We defined the blue HB stars as $0 < V - I < 0.38, 21.88 < V < 22.48$ stars and the red HB stars as $0.58 < V - I < 0.88, 21.88 < V < 22.38$ and $V > -0.4/0.16[(V - I) - 0.58] + 22.08$. See Fig. 4 for these criteria in detail. To identify RGB stars, we determined the mean RGB sequence which was fitted as,

$$(V-I)_{RGB} = 197.717-33.592V+2.169V^2-6.267\times10^{-2}V^3+6.830\times1 \quad (1)$$

Fig. 4 (a) shows how well the mean RGB sequence traces the data. The stars that deviate less than ±0.075 mag (corresponding to 2.3σ) in $V - I$ color from the mean RGB sequence are classified as RGB stars. The criteria enclose most of the RGB stars and separate red HB stars fairly well. We set the faint limit of the RGB at $V = 23.5$ to avoid contamination from foreground stars and unresolved background galaxies, as well as to be free from the completeness correction. The RGB stars were subdivided into bright and faint RGB stars at the HB level ($V_{HB} = 22.18$, Mighell & Rich 1996).

We compared the mean RGB sequence with those of Galactic globular clusters M 15, NGC 6397, M 2, and NGC 1851 taken from da Costa & Armandroff (1990) in Fig. 4 (b). These clusters have metallicities [Fe/H] of -2.17, -1.91, -1.58, and -1.29, respectively (da Costa & Armandroff 1990). The mean RGB sequence of Leo II lies in between NGC 6397 and M 2, suggesting that the mean metallicity of Leo II would be between -1.91 and -1.58 if an old stellar population as Galactic globular clusters is assumed. This value is consistent with those derived spectroscopically by Bosler et al. (2004) and Koch et al. (2007). The mean RGB sequence we obtained is slightly bluer than that derived by Mighell & Rich (1996). Their mean RGB sequence is just on the M 2 RGB sequence. A likely cause of this could be the difference in the size of the survey field and will be discussed further in Sect. 5.

We counted the number of stars in each stellar component (i.e., bright and faint RGB, blue and red HB) in an annular area of $r_{in} < r < r_{out}$ and divided this by the area of the annulus to derive the number density. The characteristic radius $< r >$ for an annulus is defined as,

$$\int_{r_{in}}^{<r>} dA = \int_{<r>}^{r_{out}} dA \quad (2)$$

$$\langle r \rangle = \sqrt{(r_{out}^2 + r_{in}^2)/2} \quad (3)$$

In Fig. 5 the radial profiles for each stellar component are plotted as a function of the characteristic radius. The numbers are listed in Tab. 2. We fitted the radial profile for each stellar component with the King profile and listed the best-fit parameters in Tab. 3. The core and tidal radii calculated for all RGB stars are 2.76 arcmin and 8.63 arcmin, respectively, and are consistent with those derived by Irwin & Hatzidimitriou (1995). Bright RGB stars are slightly more concentrated than faint RGB stars in terms of the core radius. This is also confirmed by a cumulative number fraction plot shown in the inset

of Fig. 5. We calculated the KS probabilities that two different stellar components had the same spatial distribution. The probabilities are less than 1% except for the pair of bright RGB and red HB stars (76.3%). The King profile fitting for bright RGB stars is achieved for $r < 9$ arcmin, as suggested by the best-fit tidal radius of 9.22 arcmin, and the number density of bright RGB stars shows the shallower slope for $r > 9$ arcmin and a probable drop at $r > 14$ arcmin. A similar trend is also seen for faint RGB stars, and the change in the slope occurs at $r \sim 8.5$ arcmin (c.f., the best-fit tidal radius of 8.51 arcmin), although the number density may reach the field level at $r > 11$ arcmin.

The field contamination is estimated in the following way. Ratnatunga & Bahcall (1985) calculated the number of field stars with different colors toward the direction of Leo II. The number of field stars with $(B-V) < 0.8$ and $19 < V < 22.18$ is estimated to be 0.14 arcmin^{-2} based on their table. Considering that the color of $(B-V) = 0.8$ corresponds to a K0V star and hence, $(V-I) = 1.87$, and that most field stars are redder than $(V-I) = 0.6$, we expect 0.14 arcmin^{-2} field stars in the color range of $0.6 < (V-I) < 1.87$. We therefore estimated that 0.0165 arcmin^{-2} field stars are in our bright RGB selection criteria ($19 < V < 22.18$ and $\Delta(V-I) = 0.15$). We also estimated the number of field stars using the SDSS DR5 archive data (Adelman-McCarthy et al. 2007). The bright RGB selection criteria were determined on the basis of the (g, i) color-magnitude diagram of Leo II and the number of stars within the criteria in the nearby field of Leo II (1 degree from Leo II) was determined. The estimated field contamination is 0.0226 arcmin^{-2}, which is consistent with that determined above. We therefore conclude that the number of field contaminations for the bright RGB stars is ~ 0.02 arcmin^{-2} and that stars located at $r > 14$ arcmin are likely to be dominated by the field population. Adopting this field contamination number, we suggest that the shallower slope of the radial profile found for $9 < r < 13$ arcmin is real. The field contamination for faint RGB stars is expected to be smaller than ~ 0.02 arcmin^{-2} because of the smaller magnitude coverage of the selection criteria, but contamination from background compact galaxies that are misclassified as stars may occur. The SDSS data are too shallow to be used for estimating the field contamination. If stars found for $r > 14$ arcmin consist of such a mixture of field contamination and the background compact galaxies as implied from the analysis for the bright RGB stars, the shallower slope found for $8 < r < 11$ arcmin is also suggested to be real.

To further investigate the details of the extra-tidal structure, we made a smoothed surface brightness map for the entire survey field as follows. Stars regarded as RGB or HB stars were listed and Gaussians of 1 arcmin kernel multiplied by the luminosity of each star was placed at the position of each star. They were then coadded to obtain a smoothed surface brightness map. This operation makes hidden faint structures clearer. Fig. 6 is the resuling smoothed surface brightness map. The isosurface-brightness contour of the bright part of the galaxy is almost circular, but it becomes more complicated at a lower surface brightness. The most remarkable feature of Fig. 6 is the diffuse knotty structure prominent in the eastern part of the galaxy ($\Delta\alpha \sim =$ -11, $\Delta\delta \sim 1$). The knot is more than five times more luminous than the position located at the same distance from the center at the opposite side of the galaxy, although the mean surface brightness is quite faint (~ 31 mag/arcsec^{-2}). The knot contains four bright RGB stars in $\simeq 4 \times 5$ arcmin^2 area and the expected field contamination number is 0.4, indicating that the knot is 99.92% significant above the field population on the basis of Poisson statistics.

The extent of this knot is about 4 arcmin (270 pc in physical size) with a width of 2.5 arcmin (170 pc), and it is small compared to the main body of Leo II. The magnitude of this knot was estimated to be $M_V = -2.8$ by summing up luminosities of 15 stars found in the knot region that are brighter than $V = 23.5$. The value is close to the magnitude of the least luminous globular cluster. The knot must be more luminous because we neglected a contribution from underlying faint stars, and could be more luminous if it is indeed extended farther to the east (out of our survey field), or if the main part of it is already merged with the main body of Leo II. It is possible that the substructure is a small globular cluster that is being disrupted and merging into the main body of Leo II. The other possibility is that the knot is composed of stars stripped from the main body of Leo II. The origin of the substructure is discussed further in Sect. 7.

4. HORIZONTAL BRANCH MORPHOLOGY

In brief, the HB morphology indicates a distribution in the color of HB stars. It is often parameterized as $(B-R)/(B+V+R)$, where B and R are the numbers of blue and red HB stars, respectively, and V is the number of stars lying on the RR Lyr instability strip. Intensive investigation on the HB morphology of globular clusters has shown that it depends primarily on metallicity in that less metal-rich systems show a bluer HB morphology, but it is also influenced by the *second parameter*, which is most likely to be age (Lee, Demarque & Zinn, 1994). The HB morphology is thus a key measure in studying the properties of stellar populations and the variation in the HB morphology within a galaxy is often investigated (e.g., Harbeck et al. 2001; Tolstoy et al. 2004). Using our data, we can examine the detailed variation of the HB morphology over a wide radius from the center to far beyond the tidal radius of Leo II.

Fig. 7 shows the HB morphology index $(B-R)/(B+V+R)$ plotted as a function of the radius. The index is less than zero at any radius, indicating that red HB stars are more numerous than blue HB stars everywhere in Leo II. This value agrees with those obtained in other studies (-0.68, Demers & Irwin 1993; -0.78 ± 0.10, Mighell & Rich 1996). The index is small at the center of the galaxy and becomes larger as the radius increases for $r > 3$ arcmin, reaching its maximum at $r = 6$ arcmin. The trend is consistent with the findings of da Costa et al. (1996). They showed that the HB morphology index is approximately constant out to $r \simeq 3$ arcmin but the fraction of blue HB stars increases beyond $r \simeq 3$ arcmin. This means that red HB stars are more concentrated to the center than blue HB stars for $r < 6$ arcmin. The inset of Fig. 7, which presents the cumulative number fraction of blue and red HB stars as a function of the radius, clearly shows this and confirms the result of Bellazzini et al. (2005; see their Fig. 8). They suggest that age is

the main driver of the population gradient. Koch et al. (2007) support this suggestion although they did not detect any considerable metallicity or age gradient in Leo II. The trend of a centrally-concentrated red HB distribution is also observed in many dwarf spheroidal galaxies in the Local Group (Majewski et al. 1999; Harbeck et al. 2001; Tolstoy et al. 2004). Our results support the idea that the radial gradient of the HB morphology is common to dwarf spheroidal galaxies.

For the outer part of the galaxy ($r > 7$ arcmin), the HB morphology index looks almost constant at $(B-R)/(B+V+R) \sim -0.6$, and the value is larger than that at the inner part ($r < 5$ arcmin). This means that blue HB stars are more numerous, implying that the stellar population in the outer region is less metal-rich and/or older than those in the inner part.

5. BLUE/RED RGB DISTRIBUTION

We investigated the color distribution of the RGB stars. In an analogy to the HB morphology index, we used the RGB color index for the analysis, defined as $(B-R)/(B+R)$, where B and R are the numbers of stars that deviate less than 0.075 mag bluer and redder from the mean RGB sequence, respectively (see also Fig. 4). The mean RGB sequence is defined as Eq. 1, and those stars $19 < V < 23.5$ were used. Since the AGB merges to the RGB from the blue side to to the bright part of the RGB, it is possible that the RGB color index may not have been determined correctly due to the contamination of AGB stars, especially when the number fraction of AGB stars to RGB stars is large. To estimate the influence of AGB stars in the determination of the index, we derived the RGB color index using whole RGB stars ($19 < V < 23.5$) and faint RGB stars ($22.18 < V < 23.5$). We plotted the results as open triangles (whole RGB) and filled squares (faint RGB) in Fig. 8. The color index derived from whole RGB stars at a fixed radius is slightly larger (i.e., bluer color) than that derived from faint RGB stars, indicating an influence, albeit small, of AGB stars. Therefore, the RGB color index is more accurately derived by using faint RGB stars ($22.18 < V < 23.5$).

The color index is distributed around zero at any radius except for the center where red RGB stars seem to be numerous. This fact gives a reasonable explanation for the color difference of the mean RGB sequence between this study and the redder mean RGB color of Mighell & Rich (1996). Since their survey was limited to a small area (4.44 arcmin^2) at the galaxy center, they inevitably sampled red RGB stars, which are numerous at the center, and hence obtained a redder mean RGB color. This also suggests that the stellar population varies within a galaxy.

The inset of Fig. 8 shows the cumulative number fraction of both blue and red RGB stars. The radial distribution is quite similar between the blue and red RGB stars, in contrast to the same figure for blue and red HB stars (Fig. 7). However, the coincidence of the RGB color indices of the two stellar groups does not always mean that the stellar populations of two groups are identical. For example, the color index cannot distinguish between broad and narrow color distributions around the mean RGB sequence; thus, examining the color distributions around this sequence is of key importance, as shown in Fig. 9. Here we divided the stars into four groups according to radius, $r < 1'.5$, $1'.5 < r < 3'.0$, $3'.0 < r < 6'.7$ and $6'.7 < r$, and made a color histogram for each group. The figure shows that the color distribution is generally broad, but varies as the radius changes. It appears that the color distribution for $r < 3'.0$ is very broad, suggesting that the stellar population at the galaxy center is not simple and is a mixture of several stellar populations of different ages and metal abundance. This is consistent with the results of Mighell & Rich (1996), who noted the wide age spread ($\sim$ 7Gyr) for the stellar population at the center. The color distribution becomes more concentrated to $\Delta(V-I) = 0$ for $r > 3.0$ arcmin. This would imply that the stellar population for $r > 3.0$ arcmin is more homogeneous compared to that for $r < 3.0$ arcmin. [11].

6. RADIAL GRADIENT OF AGE DISTRIBUTION

Mighell & Rich (1996) derived the age distribution of the stellar population in the center of the galaxy on the basis of the magnitude distribution of subgiant branch (SGB) stars. Fig. 4 (c) focuses on the color-magnitude diagram around the bottom of the RGB and the turn-off point. The green lines represent Padova isochrones for ages 5, 10, and 15 Gyr and metallicity Z=0.0004 (Girardi et al. 2002). As shown in the figure, the isochrones are almost parallel to the $V-I$ axis (i.e., constant V magnitude) at the SGB ($V-I \simeq 0.7$), indicating that the magnitude at a fixed $V-I$ color can be translated to age. The difference in metallicity also affects the shape of the isochrone, but small differences in metallicity (e.g. Z=0.001, shown as magenta lines in Fig. 4 (c)) do not change the shape significantly. Since it is unlikely that metal rich population ($Z > 0.004$) dominates the stellar population in Leo II as suggested by the shape of mean RGB sequence, we can estimate the age distribution using the magnitude distribution of SGB stars. We examined the magnitude distribution of stars with $23.5 < V < 25.5$ and $0.67 < V-I < 0.77$, which we call SGB. The region in the color-magnitude diagram is shown as a cyan box in Fig. 4 (a) and (c).

A difficulty, however, occurs in applying this method to our data; the error in color becomes larger than the width of the selection criteria, $0.67 < V-I < 0.77$, for $V > 24.5$. This increases the uncertainty in the number estimation of SGB stars fainter than $V = 24.5$. Nevertheless, we were able to obtain a clue as to the age distribution in the following way. The key lies in the brighter SGB stars ($V < 24.5$), which indicate the presence of a younger stellar population. We can estimate what fraction of the total stellar population the young population accounts for by comparing the number ratio of bright SGB stars to faint RGB stars with a theoretical calculation. We therefore investigated the number ratio of SGB stars to faint RGB stars as a function of the radius.

To derive the number of SGB stars, the incompleteness of the detection and contaminations from unresolved background galaxies and the foreground stars must be properly corrected. We estimated the incompleteness for

[11] Note that a narrow color distribution does not necessarily imply a homogeneous stellar population (e.g., Smecher-Hane et al. 1994)

every 0.5 mag grid in the V and I bands and for 1 arcmin in radius using real images as explained in Sect. 2. Fig. 10 shows the completeness as a function of magnitude in the V and I bands at different radii (r = 0, 2.5, 5.0, 10.0 arcmin). With this incompleteness table in hand, the incompleteness at a given V magnitude, color (i.e., I magnitude, once V magnitude is given), and radius is estimated by a linear interpolation. The numbers of SGB stars are corrected for incompleteness calculated above. To estimate the number of contaminations, we regarded stars found at $r > 16.67'$ as contaminations, and the magnitude distribution of (incompleteness-corrected) contaminations with $0.67 < V - I < 0.77$ were fitted to the 4th order polynomials as, $C(arcmin^{-2}/0.1mag) = -33245 + 5448.7V - 334.59V^2 + 9.1314V^3 - 0.093365V^4$. To derive the number of SGB stars in a given annulus, the contamination number function C multiplied by the area of the annulus wa subtracted from the incompleteness-corrected number.

The number ratios of SGB stars to faint RGB stars are plotted in Fig. 11 as a function of the radius. In the figure, the number ratios are plotted separately for bright SGB stars ($23.5 < V < 24.0$, filled squares) and intermediate SGB stars ($24.0 < V < 24.5$, open triangles). Note that $23.5 < V < 24.0$ and $24.0 < V < 24.5$ populations roughly correspond to $2.5 \sim 4$ Gyr and $4 \sim 6.3 - 8$ Gyr populations, respectively. We noted that the number ratios for both bright and intermediate SGB stars increase toward the center of the galaxy. The slope is steeper for intermediate SGB stars.

The number ratio can be calculated theoretically for a stellar population of fixed age and metallicity using Padova isochrones and the initial mass function. We adopted Salpeter's form for the initial mass function. The calculation shows that the number ratios for bright SGB stars ($23.5 < V < 24.0$) range $0.37 \sim 0.41$ for Z=0.0004 population stars. If a stellar population is dominated by a Z=0.0004 population, the number ratio should be close to the value. The number for a Z=0.001 population ranges $0.66 \sim 0.76$. Although the calculated values are different according to the adopted metallicity, the number ratios at any radius are well below all the calculated values. This indicates that a population younger than 4 Gyr is not a dominant population, although it certainly resides in the galaxy center. The existence of a stellar population as young as 2 Gyr reported by Bosler et al. (2004) and Koch et al. (2007) also supports our finding. The increase in the number ratio at the galaxy center suggests that (1) the fraction of the young population is higher at the center than at the periphery, (2) the metallicity of the young population is higher at the center than at the periphery, or (3) a combination of (1) and (2).

For intermediate SGB stars ($24.0 < V < 24.5$), the calculated number ratios range $0.5 \sim 0.8$ and $0.6 \sim 1.0$ for Z=0.0004 and Z=0.001 populations, respectively. The number ratio is ~ 0.7 at the center and ~ 0.5 within 3 arcmin from the center, indicating that an intermediate age population ($4 \sim 8$ Gyr) is dominant at the galaxy center. This is consistent with the finding by Mighell & Rich (1996) and Dolphin (2002) that a considerable stellar population younger than 8 Gyr occurs at the center of Leo II. However, the number ratios of both bright and intermediate SGB stars become small as the radius increases, indicating that the stellar population at the outskirts of the galaxy is deficient in young population, i.e., most of the stars are older than 8 Gyr.

7. THE EVOLUTION OF LEO II

7.1. *Main Body*

The stellar population in the outskirts of the galaxy ($5 \lesssim r \lesssim r_t$) was shown to consist of mostly older stars ($\gtrsim 8$ Gyr). If metal abundance is nearly homogeneous, such an old population must form a narrow color distribution at the RGB, which is confirmed by a concentrated distribution in $V-I$ color of faint RGB stars as shown in Fig. 9. A comparison of Padova isochrones with the color distribution of RGB stars in the outskirts suggests low-metal-abundance populations (between Z=0.0004 and Z=0.001) in the outskirts if ages of $10 \sim 15$ Gyr are assumed. The larger HB morphology index (Fig. 7) also supports an old population with low metal abundance. We conclude that the dominant population in the outskirts of the galaxy is an old population with low metal abundance.

The stellar population at the center of the galaxy, however, shows a variety of age. It is necessary to include stars younger than 10 Gyr, but a young population with low metal abundance, for example, $\lesssim 10$ Gyr and Z=0.0004 population, is excluded since the isochrone would not trace the RGB distribution. Therefore, a higher metal abundance ($Z \simeq 0.001$, possibly $Z \simeq 0.004$ for very young population) is suggested.

From the foregoing results, Leo II is suggested to have evolved as follows. Leo II first started to form stars over the whole galaxy about 15 Gyr ago[12] with a modest (probably low) star-formation rate. Star formation lasted for some time and the interstellar gas gained metals. Then about 8 Gyr ago, star formation began to cease from the outskirts and the star-forming region gradually became more concentrated to the center. The star-forming activity had dropped to ~ 0 by ~ 4 Gyr ago, except for the center where a small population younger than 4 Gyr occurs.

Hensler et al. (2004) demonstrated the one-dimensional chemodynamical evolution of dwarf elliptical galaxies, and showed the interesting feature that the star-forming region shrinks as a galaxy evolves because of gas exhaustion in the galaxy. Their simulation seems to outline the evolution of Leo II fairly well, although it requires a refinement to fully explain our results. Since a population gradient within a galaxy is also observed for several Local Group dwarf spheroidal galaxies (e.g., Harbeck et al. 2001), a more refined chemodynamical model will be necessary to explain the population gradient in the future to clarify the evolution of dwarf spheroidal galaxies.

7.2. *Halo Structure*

The origin of the knotty substructure found at the extended halo of Leo II could be (1) a small globular cluster, which is disrupted and merged with the main body of Leo II, (2) stars stripped from the main body of Leo II, or (3) a foreground artifact. The properties of stellar populations such as HB morphology are almost the same

[12] This estimate is based on the oldest ages in the adopted isochrone grids.

between outside the tidal radius and at the outskirts of the main body, indicating that the knot would be dominated by old stars with low metal abundance. To further investigate the stellar population of the knot, we made a Hess diagram from which field contaminations were statistically subtracted. In Fig. 12, although the field subtraction is not perfect, two significant concentrations of stars are observed around the red clump ($V-I \sim 0.8$, $V \sim 22$) and the turn-off point ($V-I \sim 0.7$, $V \sim 26$) like that seen in Fig. 3. This suggests that the knot is likely to consist of a similar stellar population as that residing in the outskirts of Leo II and the probability of (3) is low. However, based on this figure, it is still difficult to determine whether possibility (1) or (2) is more likely.

If the second scenario is true, the tidal influence of the Galaxy would be the most efficient mechanism to strip stars from the main body of Leo II. Indeed, many dwarf spheroidal galaxies such as Draco and Ursa Minor are now known to host extra-tidal halo structures although they are closer to the Galaxy and hence more influenced by the Galactic tidal force. However, the present-day remote location of Leo II from the Galaxy raises the question of whether the tidal force of the Galaxy is enough to strip stars from the main body of Leo II. In addition, the fact that we do not detect any obvious extra-tidal structure at the opposite side of Leo II is unfavorable for this scenario. Therefore, it is unlikely that tidally stripped stars are the origin of the knotty substructure. If the knot is indeed a result of the tidal stripping, it should be aligned to the direction parallel to the motion of Leo II. Therefore, measuring the proper motion of Leo II would provide a clue to answering this problem, although it would still be quite challenging.

The fact that no globular clusters are found to associate with less luminous dwarf spheroidals such as Leo II does not support the first scenario for the origin of the knot. But it is possible that Leo II formed together with a small number of globular clusters and we may be watching the disruption process of the last one that happened to survive until the recent past. It is interesting that Kleyna et al. (2003) demonstrated the survival of a substructure for a Hubble time in a cored dark-matter halo. They suggested that the substructures found in Ursa Minor are the remnants of a disrupted stellar cluster and that Ursa Minor possesses a cored dark-matter halo. Following their idea, we suggest that Leo II may be another example of a galaxy with a cored dark-matter halo.

Recent numerical simulations suggest that dark halos of dwarf spheroidals are larger than previously thought, and hence, extra-tidal stars are gravitationally bound to the galaxies and are a part of the extended stellar halos (Hayashi et al. 2003; Mashchenko et al. 2005). The extended halo structure found in this study might be a structure bound to Leo II according to the predictions of the simulations.

8. SUMMARY

We carried out a wide-field imaging survey of the Local Group dwarf spheroidal galaxy Leo II in the V and I bands using Suprime-Cam on the 8.2-m Subaru Telescope. The survey covered an area of 26.67×26.67 arcmin^2, far beyond the tidal radius of the Leo II (8.63 arcmin). A total of 82252 stars was detected down to the limiting magnitude of $V \simeq 26$, which is roughly 1 mag deeper than the turn-off point of the main sequence stars of Leo II. Our main conclusions are summarized below.

- The radial number density profile of bright RGB stars is shown to continue beyond the tidal radius ($r_t = 9.22$ arcmin). A change in the slope occurs near the tidal radius and the slope becomes shallower for $r > 9$ arcmin. A hint of a drop is seen in number density at $r > 14$ arcmin. A similar two-component profile is also observed for faint RGB stars.

- A smoothed surface brightness map of Leo II suggests the existence of a small substructure beyond the tidal radius, which is as large as globular clusters in luminosity ($M_V < -2.8$). It could possibly be a disrupted globular cluster of Leo II that had survived until the recent past. Another possibility is that it is composed of stars stripped from the main body of Leo II, although this is unlikely.

- The HB morphology index shows a radial gradient in the sense that red HB stars are more concentrated than blue HB stars. Such a trend is also observed in several Local Group dwarf spheroidal galaxies. The HB morphology index implies that the stellar population in the outer part ($r > 7$ arcmin) is more metal-poor and/or older than that in the inner part.

- The RGB color index is almost constant at any radius except for the center, where a redder mean RGB sequence than ours was observed by Mighell & Rich (1996). The color distribution of RGB stars around the mean RGB sequence shows a broader distribution at the center ($r < 3$ arcmin) than the outskirts. This suggests a more homogeneous stellar population at the outskirts of the galaxy and a variety of stellar populations at the galaxy center.

- The age distribution was estimated using brighter ($23.5 < V < 24.5$) SGB stars. The presence of a younger stellar population than 4 Gyr is suggested for the center, although it is not a dominant population. The contribution of an intermediate-age ($4 \sim 8$ Gyr) stellar population seems to be considerable at the galaxy center, but the contribution of such a population is small at the outskirts.

- The evolution of Leo II is suggested to be as follows. (1) Leo II first began forming stars throughout the whole galaxy with a constant (inefficient) star-formation rate. (2) The star formation then began to cease in the outskirts and the star-forming region gradually shrank toward the center. (3) The star-forming activity had dropped to ~ 0 by ~ 4 Gyr ago except at the center, where a small population younger than 4 Gyr is found.

We thank the observatory staff of the Subaru Telescope for their excellent support. We are grateful to the anonymous referee for many valuable comments and suggestions which improve this paper very much.

REFERENCES

Adelman-McCarthy, J. K., et al., 2007, ApJS, submitted
Bellazzini, M., Gennari, N., & Ferraro, F. R., 2005, MNRAS, 360, 185
Bosler, T. L., Smecker-Hane, T. A., Cole, A., & Stetson, P. B., 2004, Origin and Evolution of the Elements, ed. A. McWilliam and M. Rauch, 5
Cowie, L. L., Songaila, A., Hu, E. M., Cohen, J. G., 1996, AJ, 112, 839
Coleman, M., da Costa, G. S., Bland-Hawthorn, J., Martínez-Delgado, D., Freeman, K. C., Malin, D., 2004, AJ, 127, 832
Coleman, M., da Costa, G. S., Bland-Hawthorn, J., Freeman, K. C., 2005, AJ, 129, 1443
da Costa, G. S., & Armandroff, T. E., 1990, AJ, 100, 162
da Costa, G. S., Armandroff, T. E., Caldwell, N., & Seitzer, P., 1996, AJ, 112, 2576
Demers, S., & Irwin, M. J., 1993, MNRAS, 261, 657
Dolphin, A. E., 2002, MNRAS, 332, 91
Girardi, L., et al., 2002, A&A, 391, 195
Grebel, E. K., 2000, ESA SP, 445, 87
Grebel, E. K., Gallagher, J. S.,III, 2004, ApJ, 610, L89
Harbeck, D., et al., 2001, AJ, 122, 3092
Hayashi, E., Navarro, J. F., Taylor, J. E., Stadel, J., Quinn, T., 2003, ApJ, 584, 541
Held, E. V., Saviane, I., Momany, Y., Carraro, G., 2000, ApJ, 530, L85
Hesnler, G., Theis, C., Gallagher, J. S. III., 2004, A&A, 426, 25
Irwin, M., Hatzidimitriou, D., 1995, MNRAS, 277, 1354
Kleyna, J. T., Geller, M. J., Kenyon, S. J., Kurtz, M. J., Thorstensen, J. R., 1998, AJ, 115, 2359
Kleyna, J. T., Wilkinson, M. I., Gilmore, G., Evans, N. W., 2003, ApJ, 588, L21
Kleyna, J. T., Wilkinson, M. I., Evans, N. W., Gilmore, G., 2004, MNRAS, 354, L66
Koch, A., et al., 2006, AJ, 131, 895
Koch, A., et al., 2007, AJ, 133, 270
Lee, M.-G., 1995, AJ, 110, 1155
Lee, Y.-W., Demarque, P., & Zinn, R., 1994, ApJ, 423, 248
Majewski, S. R., Siegel, M. H., Patterson, R. J., & Rood R. T., 1999, ApJ, 520, L33
Majewski, S. R., et al., 2005, AJ, 130, 2677
Martínez-Delgado, D., Gallart, C., Aparicio, A., 1999, AJ, 118, 862
Mashchenko, S., Couchman, H. M. P., Sills, A., 2005, ApJ, 624, 726
Mateo, M. L., 1998, ARA&A, 36, 435
Mighell, K. J., & Rich, R. M., 1996, AJ, 111, 777
Miyazaki, S., Komiyama, Y., Sekiguchi, M., Okamura, S., Doi, M., Furusawa, H., Hamabe, M., Imi, K., Kimura, M., Nakata, F., Okada, N., Ouchi, M., Shimasaku, K., Yagi, M., & Yasuda, N., 2002, PASJ, 54, 833
Palma, C., Majewski, S. R., Siegel, M. H., Patterson, R. J., Ostheimer, J. C., Link, R., 2003, AJ, 125, 1352
Ratnatunga, K. U., Bahcall, J. N., 1985, ApJS, 59, 63
Saviane, I., Held, E. V., Bertelli, G., 2000, A&A, 355, 966
Siegel, M. H., Majewski, S. R., 2000, AJ, 120, 284
Smail, I., Edge, A. C., Ellis, R. S., Blandford, R. D., 1998, MNRAS, 293, 124
Smecker-Hane, T. A., Stetson, P. B., Hesser, J. E., Lehnert, M. D., 1994, AJ, 108, 507
Stetson, P. B., 1987, PASP, 99, 191
Stetson, P. B., 1994, PASP, 106, 250
Tolstoy, E. et al., 2004, ApJ, 617, L119
Yagi, M., Kashikawa, N., Sekiguchi, M., Doi, M., Yasuda, N., Shimasaku, K., & Okamura, S., 2002, AJ, 123, 66
Walker, M. G., Mateo, M., Olszewski, E. W., Pal, J. K., Sen, B., Woodroofe, M., 2006, ApJ, 642, L41
Westfall, K. B., Majewski, S. R., Ostheimer, J. C., Frinchaboy, P. M., Kunkel, W. E., Patterson, R. J., Link, R., 2006, AJ, 131, 375
White, S. D. M., Frenk, C. S., 1991, ApJ, 379, 52
White, S. D. M., Rees, M. J., 1978, MNRAS, 183, 341
Wilkinson, M. I., Kleyna, J. T., Evans, N. W., Gilmore, G. F., Irwin, M. J., Grebel, E. K., 2004, ApJ, 611, L21

Band	Date	Exposure Time [sec]	FWHM [arcsec]
V	2001.4.20	3000 (5×600)	0.6 – 0.8
		900 (5×180)	0.6 – 0.8
I	2001.4.24	2400 (5×240+4×300)	0.6 – 0.8
		300 (5×60)	0.6 – 0.8

TABLE 1
The log of the observation.

Area [arcmin]	$< r >$ [arcmin]	Bright RGB	Faint RGB	Blue HB	Red HB	SB [mag/arcsec^2]
$0.0 - -0.5$	0.354	38	34	4	32	25.28
$0.5 - -1.5$	1.120	203	227	13	184	25.60
$1.5 - -2.5$	2.062	244	319	16	253	26.02
$2.5 - -3.5$	3.041	220	307	20	193	26.77
$3.5 - -4.5$	4.031	127	168	22	122	27.63
$4.5 - -5.5$	5.025	62	98	12	52	28.69
$5.5 - -6.5$	6.021	30	51	8	19	29.51
$6.5 - -7.5$	7.018	18	20	5	25	30.29
$7.5 - -8.5$	8.016	7	21	2	13	31.08
$8.5 - -9.5$	9.014	5	16	1	6	31.76
$9.5 - -10.5$	10.013	5	13	1	5	31.98
$10.5 - -11.5$	11.011	5	9	0	6	32.45
$11.5 - -12.5$	12.010	5	14	2	7	32.27
$12.5 - -13.5$	12.923	4	10	1	7	32.38
$13.5 - -$	14.215	4	18	2	9	32.97

TABLE 2
The number of stars in each area. The integrated surface brightness for these components in V band is listed in the right-most column.

	$f_{K,0}$	r_c [arcmin]	r_t [arcmin]
Bright RGB	77.6±6.5	2.28±0.30	9.22±0.53
Faint RGB	104.0±8.3	3.05±0.34	8.51±0.26
All RGB	183.4±13.2	2.76±0.28	8.63±0.26
Red HB	96.2±11.2	3.24±0.48	6.99±0.22
Blue HB	5.3±0.8	4.05±0.78	10.78±0.78

TABLE 3
The best-fit parameters for King profile fitting.

FIG. 1.— The color image of our survey area. North is to the top and east is to the left. Both width and height of the image are 26.67 arcmin.

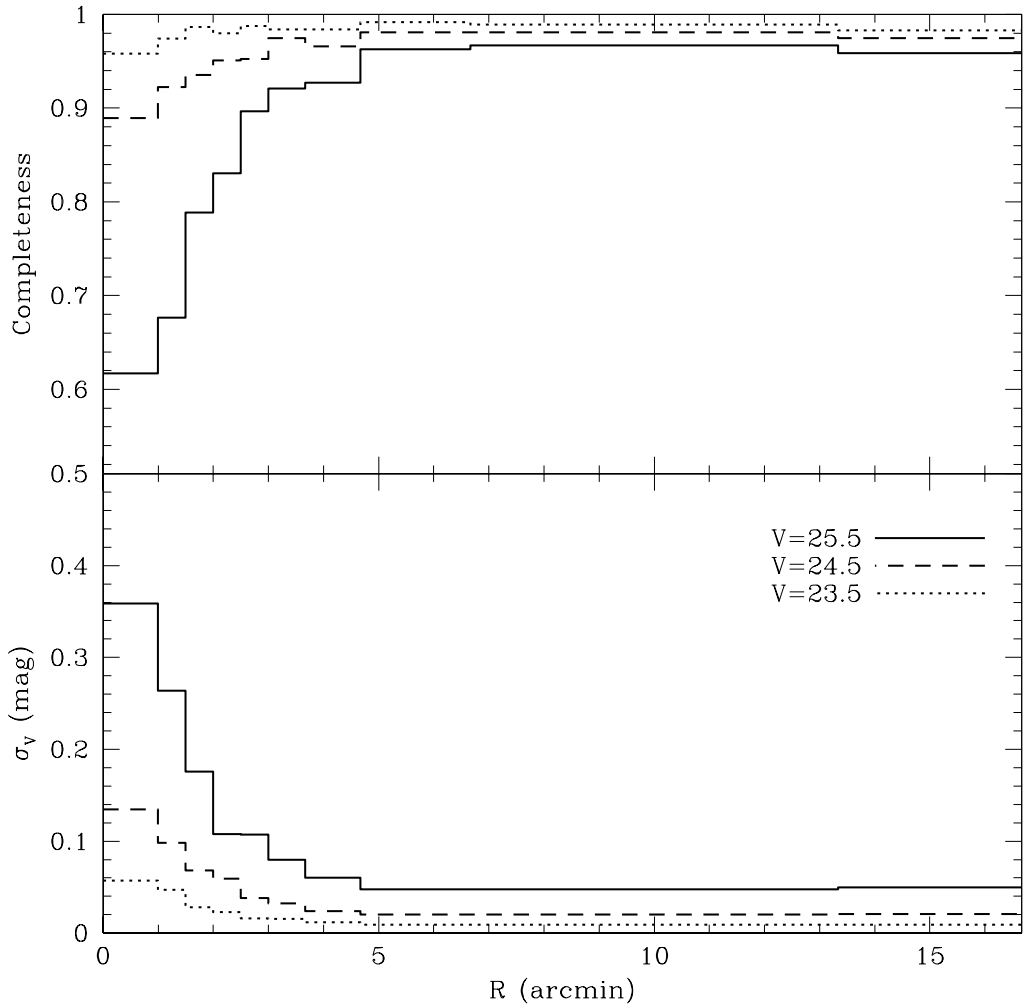

FIG. 2.— The detection completeness (top) and the magnitude errors (bottom) are plotted as a function of the distance from the galaxy center for different magnitude ($V = 23.5, 24.5, 25.5$).

FIG. 3.— The color-magnitude diagram of stars in the central 6.67×6.67 arcmin^2 field.

FIG. 4.— (a) The criteria for RGB, blue and red HB selection are overlaid on the color-magnitude diagram. Typical photometric errors at the center (~ 2.5 arcmin) and the outskirts of the galaxy are indicated as blue and red error bars at $V - I = 1.4$. (b) The detailed view of the RGB sequence. The mean RGB sequence (Eq.1) is plotted in red together with those of Galactic globular clusters M 15, NGC 6397, M 2 and NGC 1851 (from left to right) in cyan. (c) Detailed view of the SGB. Padova isochrones for ages 5, 10, and 15 Gyr (from top to bottom) of different metallicity population (Z=0.0004 in green and Z=0.001 in magenta) are overlaid.

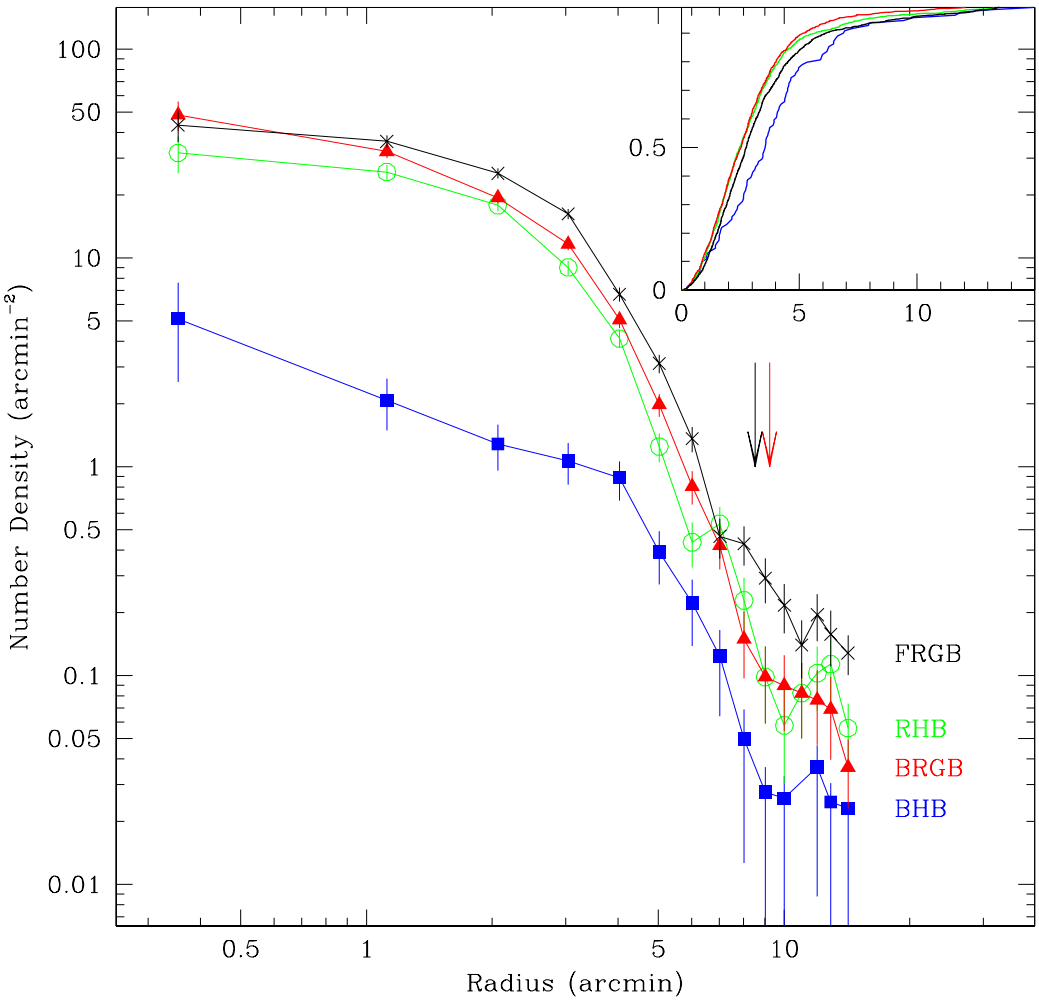

FIG. 5.— The radial profile of each stellar component. The red, black, blue and green lines represent the radial profiles of bright RGB, faint RGB, blue HB, and red HB stars, respectively. The error bars are estimated on the basis of Poisson statistics. Two arrows indicate the tidal radii calculated for bright RGB (red) and faint RGB (black), respectively. The inset shows the cumulative number fraction of each stellar component as a function of the radius in the same colors as described above.

FIG. 6.— Smoothed surface brightness map of RGB and HB stars. Contours correspond roughly to 26.5, 27.5, 28.3, 29.0, 30.0 mag/arcsec^2 from the center.

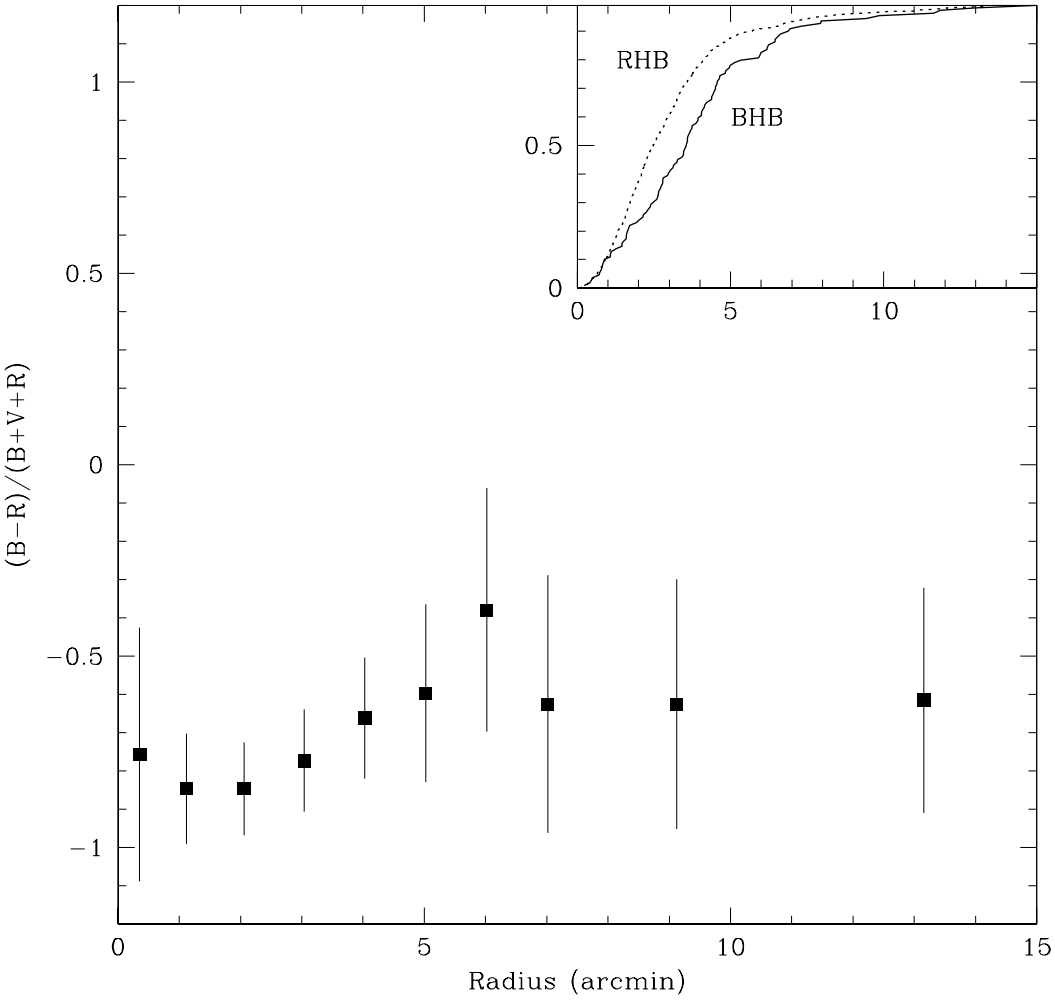

FIG. 7.— The HB morphology index $(B-R)/(B+V+R)$ plotted as a function of the radius. B, R and V indicate numbers of blue, red HB stars, and those stars found at the RR Lyr instability strip, respectively. The error bars are estimated based on the Poisson statistics. The inset shows the cumulative number fraction of blue (solid) and red (dashed) HB stars as a function of the radius.

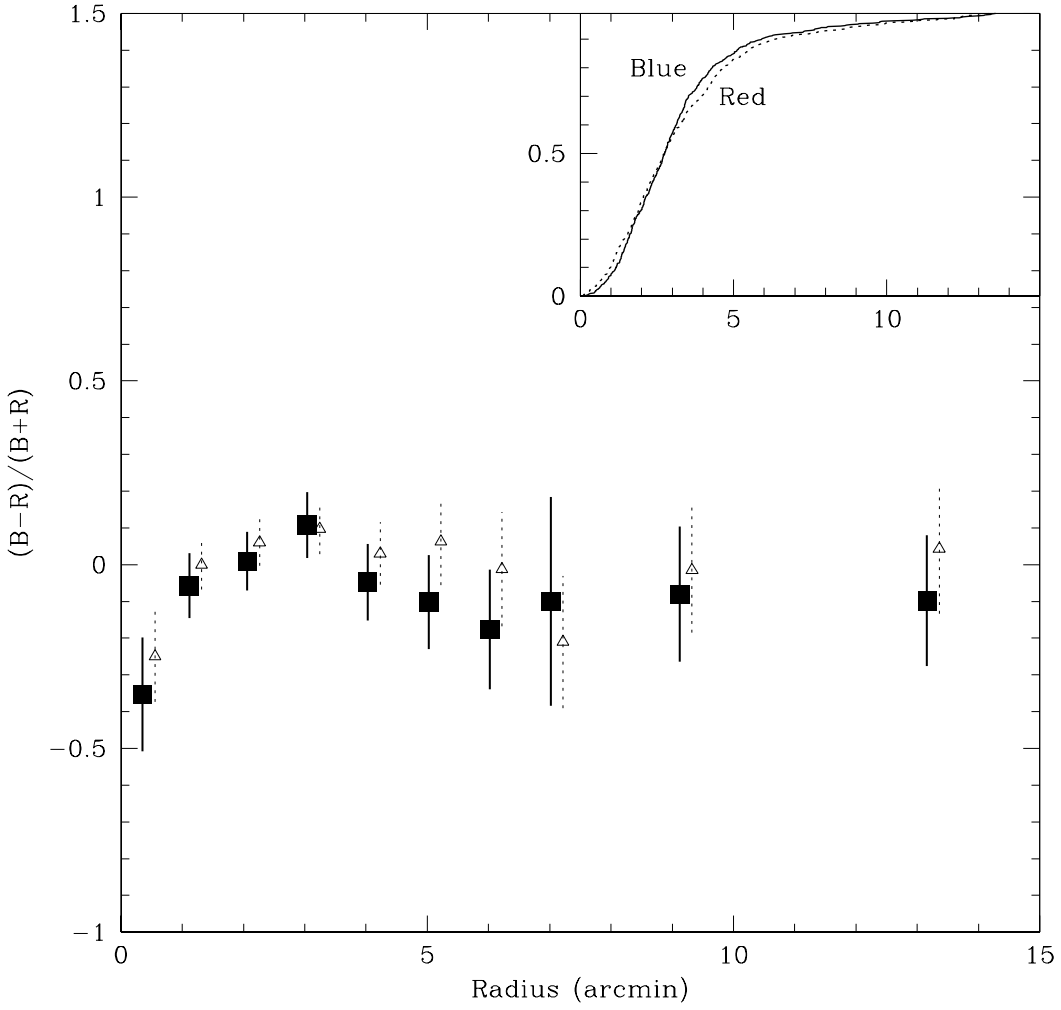

FIG. 8.— The RGB color index $(B-R)/(B+R)$ plotted as a function of the radius. B and R indicate numbers of stars that deviate less than 0.075 mag bluer and redder from the mean RGB sequence, respectively. The indices derived from whole RGB stars ($19 < V < 23.5$) and faint RGB stars ($22.18 < V < 23.5$) are plotted as open triangles and filled squares. The error bars are estimated based on the Poisson statistics. The inset shows the cumulative number fraction of blue (solid) and red (dashed) faint RGB stars as a function of the radius.

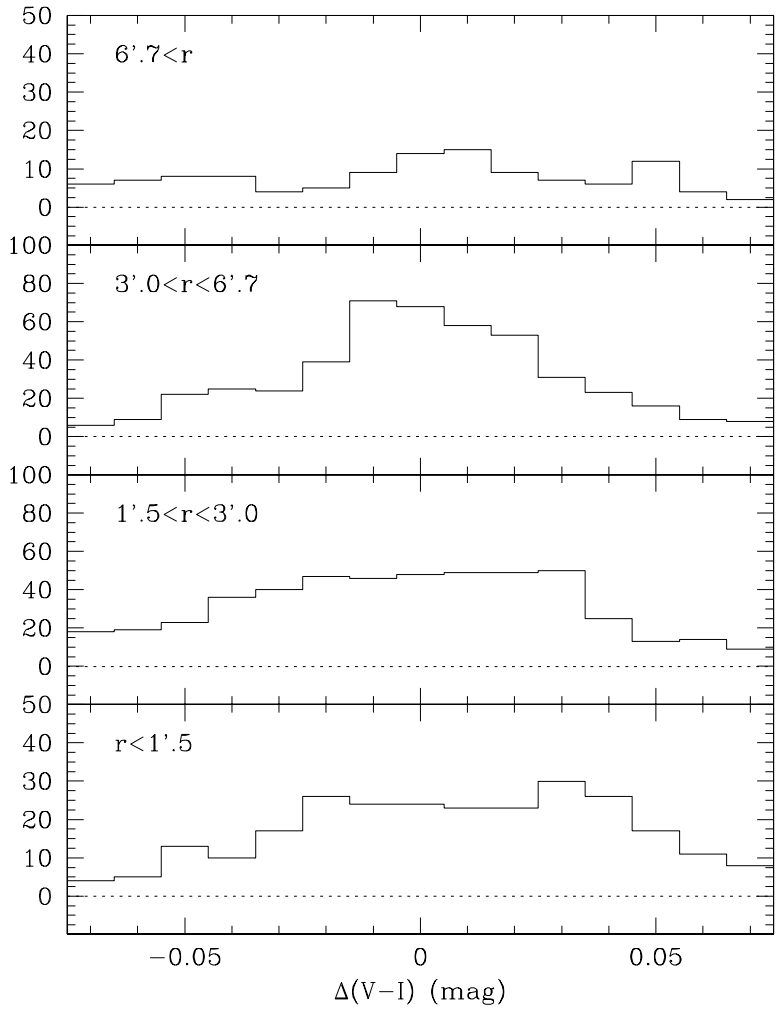

FIG. 9.— The color distribution of faint RGB stars around the mean RGB sequence in different annuli ($r < 1'.5, 1'.5 < r < 3'.0, 3'.0 < r < 6'.7$, and $6'.7 < r$).

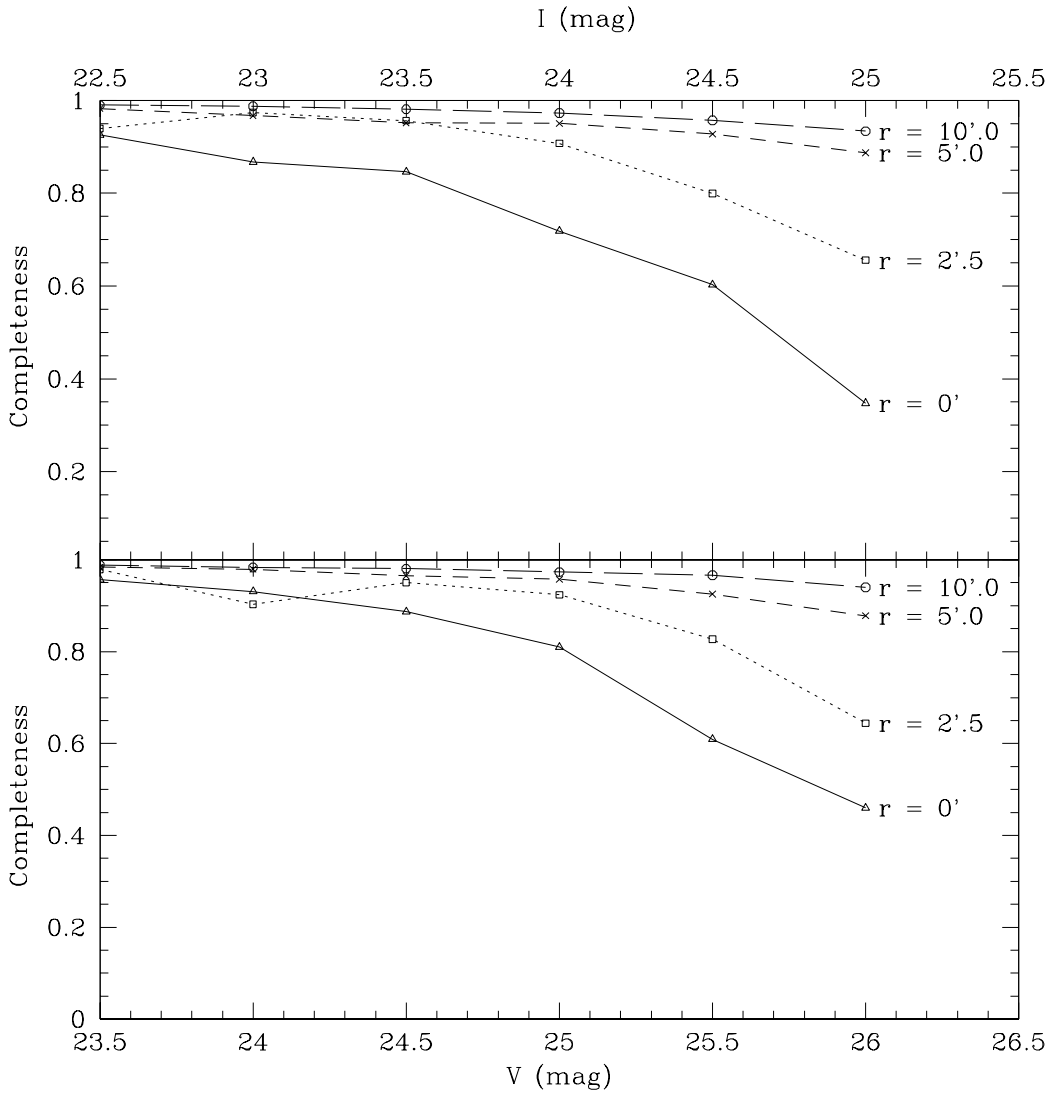

FIG. 10.— Detection completeness as a function of magnitude in V (bottom) and I (top) bands for different radii (r = 0, 2.5, 5.0, 10.0 arcmin).

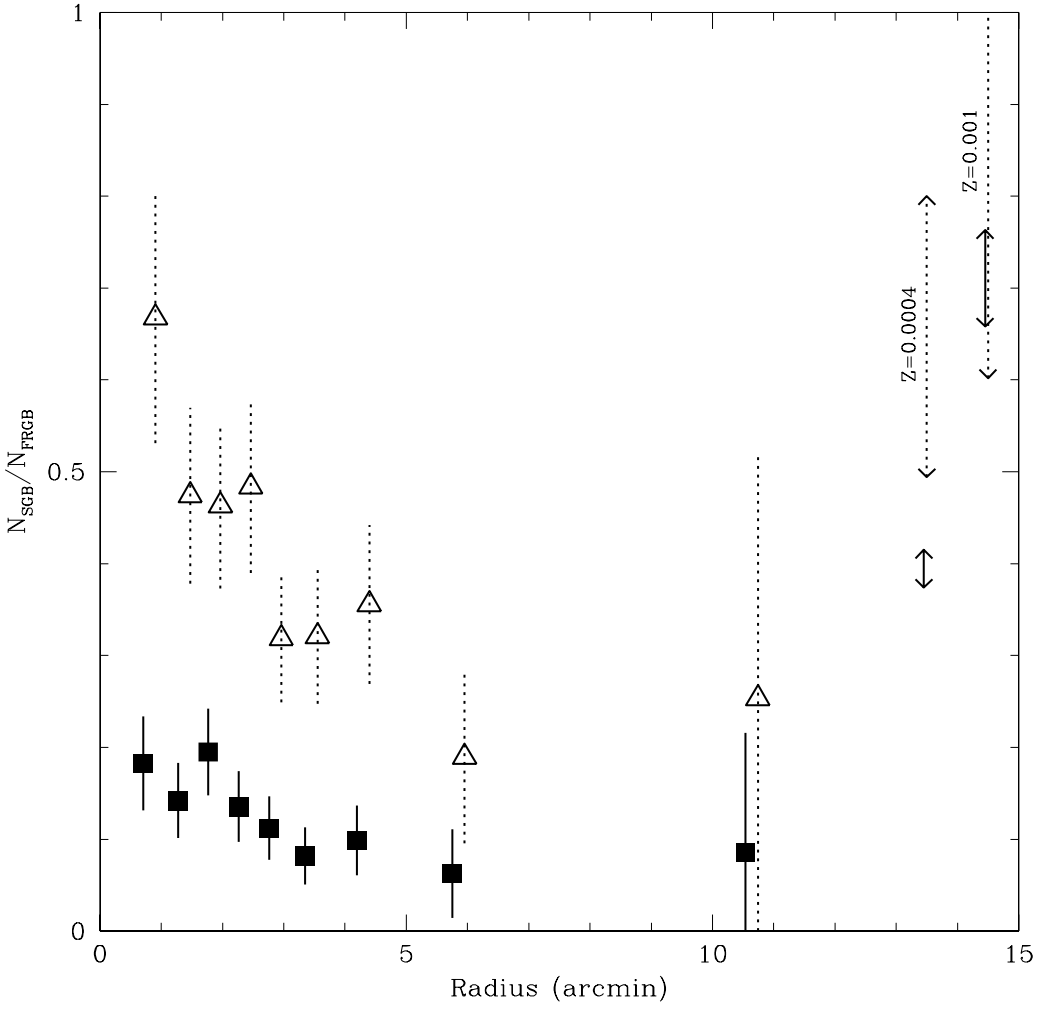

FIG. 11.— The number ratio of SGB to faint RGB stars plotted as a function of the radius. Filled squares and open triangles represent the number ratio for bright ($23.5 < V < 24.0$) and intermediate ($24.0 < V < 24.5$) SGB stars, respectively. The error bars are estimated on the basis of Poisson statistics. The solid and dotted arrows at $r \sim 14$ represent the calculated number ratios (see text) for bright and intermediate SGB stars, respectively, of different metallicities.

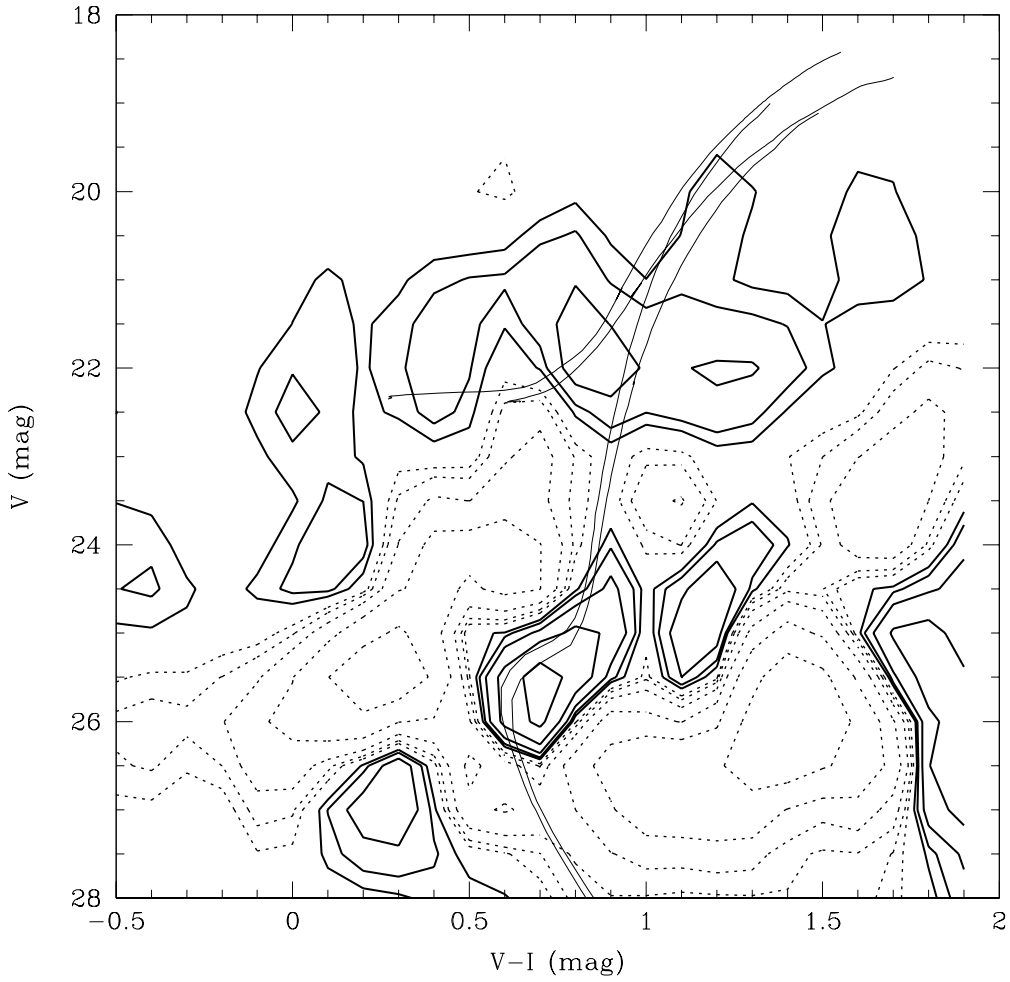

FIG. 12.— Field subtracted Hess diagram for the knot. The solid contours represent 1, 2, 4, 8, 16, 32 stars per $\Delta(V-I) = 0.1$ and $\Delta V = 0.5$ bin. The dotted contours represent -1, -2, -4, -8, -16, -32 stars, indicating that field contamination is oversubtracted. Two isochrones (Z=0.0004 and Z=0.001 with age of 15 Gyr) are overlaid for the guidance.

This figure "f1.jpg" is available in "jpg" format from:

http://arXiv.org/ps/0705.2901v1

This figure "f3.jpg" is available in "jpg" format from:

http://arXiv.org/ps/0705.2901v1

This figure "f4.jpg" is available in "jpg" format from:

http://arXiv.org/ps/0705.2901v1

This figure "f6.jpg" is available in "jpg" format from:

http://arXiv.org/ps/0705.2901v1